

Slow spin-glass and fast spin-liquid components in quasi-two-dimensional $\text{La}_2(\text{Cu},\text{Li})\text{O}_4$

Y. Chen,^{1,2,3} Wei Bao,^{1,*} Y. Qiu,^{2,3} J. E. Lorenzo,⁴ J.L. Sarrao,¹ D. L. Ho,^{2,3} and Min Y. Lin^{2,5}

¹*Condensed Matter and Thermal Physics, Los Alamos National Laboratory, Los Alamos, NM 87545*

²*NIST Center for Neutron Research, National Institute of Standards and Technology, Gaithersburg, MD 20899*

³*Dept. of Materials Science and Engineering, University of Maryland, College Park, MD 20742*

⁴*CNRS, BP 166X, F-38043, Grenoble, France*

⁵*ExxonMobil Research and Engineering Company, Annandale, NJ 08801*

(Dated: August 13, 2018)

In conventional spin glasses, magnetic interaction is not strongly anisotropic and the entire spin system is believed to be frozen below the spin-glass transition temperature. In $\text{La}_2\text{Cu}_{0.94}\text{Li}_{0.06}\text{O}_4$, for which the in-plane exchange interaction dominates the interplane one, only a fraction of spins with antiferromagnetic correlations extending to neighboring planes become spin-glass. The remaining spins with only in-plane antiferromagnetic correlations remain spin-liquid at low temperature. Such a novel partial spin freezing out of a two-dimensional spin-liquid observed in this cold neutron scattering study is likely due to a delicate balance between disorder and quantum fluctuations in the quasi-two dimensional $S=1/2$ Heisenberg system.

I. INTRODUCTION

The parent compound for high transition-temperature superconductors, La_2CuO_4 , is an antiferromagnetic insulator. Magnetic exchange interaction J between the nearest neighbor $S=1/2$ spins of Cu^{2+} ions in the CuO_2 plane is several orders of magnitude stronger than the interplane exchange interaction, making quantum spin fluctuations an essential ingredient for magnetic properties in the quasi-two-dimensional (2D) Heisenberg system^{1,2,3}. The Néel temperature T_N of La_2CuO_4 is suppressed rapidly to zero by $x_c = 2\text{--}3\%$ hole dopants such as Sr, Ba or Li^{4,5,6}, while it is suppressed with isovalent Zn substitution at a much higher concentration close to the site dilution percolating threshold of $\sim 30\%$ ⁷. The strong effect of holes has been shown to be related to induced magnetic vortices, which are topological defects in 2D systems^{8,9}. The paramagnetic phase exposed by hole doping at $T \ll J/k_B$ is dominated by zero-point quantum spin fluctuations and is referred to as a quantum spin liquid². Detailed predictions for spin dynamics have been made for the quantum spin-liquid^{2,3}.

However, in a wide doping range of $\text{La}_2\text{Cu}_{1-x}\text{Li}_x\text{O}_4$ below ~ 10 K, a spin-glass transition has been reported in muon spin rotation (μSR)⁶, nuclear quadrupole resonance (NQR)¹⁰ and magnetization¹¹ studies. A similar magnetic phase diagram has also been reported for $\text{La}_{2-x}\text{Sr}_x\text{CuO}_4$ and $\text{Y}_{1-x}\text{Ca}_x\text{Ba}_2\text{Cu}_3\text{O}_6$ ^{12,13,14,15,16,17}. In conventional spin glasses, magnetic interactions are more or less isotropic in space, and the entire spin system is believed to be frozen in the spin-glass phase¹⁸. Such was also the conclusion of a comprehensive magnetization study on $\text{La}_{2-x}\text{Sr}_x\text{CuO}_4$ ¹⁷. Although magnetization can only account for a tiny fraction of spins, theoretical pictures were proposed for spin-freezing in the whole sample^{17,19}. If the spin-glass phase in hole-doped cuprates behaved as in conventional spin-glasses, the ground state would be a spin-glass, instead of the Néel order for doping smaller than x_c , or a quantum spin

liquid for doping larger than x_c . Thus, as pointed out by Hasselmann et al.²⁰, the quantum critical point of the antiferromagnetic phase at $x_c \approx 2\text{--}3\%$ would be preempted.

In widely circulating “generic” phase-diagram for laminar cuprates, the “reentrant” spin-glass transition below the Néel temperature is generally ignored. Also generally ignored is the spin-glass transition below the superconducting transition. The spin glass phase exists side by side with the Néel order at lower doping and the superconducting order at higher doping in this neat picture. This “generic” picture does not conform to experimental results, and serves to support the theory that the spin-freezing is an extrinsic dirt effect. However, there are other theories which consider spin-freezing intrinsic to the doped cuprates^{21,22}. Physical quantities in the doping regime, including spin excitation spectra, have also been calculated from microscopic model^{23,24}.

Recently, 2D spin fluctuations in $\text{La}_2\text{Cu}_{1-x}\text{Li}_x\text{O}_4$ ($0.04 \leq x \leq 0.1$) were observed to remain liquid-like below the spin-glass transition temperature^{25,26}, $T_g \sim 9$ K, which can be reliably detected using the μSR technique⁶. The characteristic energy of 2D spin fluctuations saturates at a finite value below ~ 50 K^{25,26}, as expected for a quantum spin liquid², instead of becoming zero at T_g as for spin-glass materials^{18,27}. To reconcile these apparently contradicting experimental results, we have conducted a thorough magnetic neutron scattering investigation of $\text{La}_2\text{Cu}_{0.94}\text{Li}_{0.06}\text{O}_4$ to search for spin-glass behavior. We found that in addition to the liquid-like 2D dynamic spin correlations, the rest of spins which participate in almost 3D and quasi-3D correlations become frozen in the spin-glass transition. This partial spin freezing in the laminar cuprate is distinctly different from total spin freezing in conventional 3D spin-glass materials. The observed phase separation into spin glass and spin liquid components of *different dimensionality* sheds light on a long-standing confusion surrounding the magnetic ground state in hole-doped cuprates.

The remaining of the paper is organized as the fol-

lows. Section II covers experimental details concerning the sample and neutron scattering instrumentation. Section III covers small angle neutron scattering, which is the ideal tool to detect ferromagnetic spin clusters proposed in some theories for the spin-freezing state. Section IV covers cold neutron triple-axis measurements. The excellent energy resolution is important for this study. Finally, in Section V, we discuss and summarize our results.

II. EXPERIMENTAL DETAILS

The same single crystal sample of $\text{La}_2\text{Cu}_{0.94}\text{Li}_{0.06}\text{O}_4$ used in the previous higher energy study²⁵ was investigated in this work. $T_g \approx 8$ K was determined in μSR study⁶ and is consistent with magnetization work¹¹. The lattice parameters of the orthorhombic $Cmca$ unit cell are $a=5.332\text{\AA}$, $b=13.12\text{\AA}$ and $c=5.402\text{\AA}$ at 15 K.

Wave-vector transfers \mathbf{q} near (000) and (100) in both the $(h0l)$ and $(hk0)$ reciprocal planes were investigated at NIST using the 30 meter high resolution small angle neutron scattering (SANS) instrument at NG7, and cold neutron triple-axis spectrometer SPINS. We set the array detector of NG7-SANS to 1 and 9 m, corresponding to a q range from 0.012 to 0.39 \AA^{-1} and from 0.0033 to 0.050 \AA^{-1} , respectively. At SPINS, the (002) reflection of pyrolytic graphite was used for both the monochromator and analyzer. Horizontal Soller slits of 80' were placed before and after the sample. A cold BeO or Be filter was put before the analyzer to eliminate higher order neutron in the fixed $E_f=3.7$ or 5 meV configuration, respectively.

Sample temperature was controlled by a pumped ${}^4\text{He}$ cryostat which could reach down to 1.5 K.

III. SMALL ANGLE NEUTRON SCATTERING

Hole induced ferromagnetic exchange has been theoretically proposed in the CuO_2 plane^{19,20}. It is regarded as competing with the original antiferromagnetic exchange, thus, leading to the spin-glass transition. Although long-range ferromagnetic order has never been observed, there is the possibility of short-range ferromagnetic spin clusters which freeze in the spin-glass state in this class of spin-glass models^{19,28}. SANS has been demonstrated as a powerful tool to probe such clusters²⁷.

Two reciprocal zones of $\text{La}_2\text{Cu}_{0.94}\text{Li}_{0.06}\text{O}_4$ were studied, with incident beam parallel to the (001) or (010) direction. Therefore, any spin orientation in the sample can be detected in our experiment. The experiments were carried out at 3, 10, 15, 30 and 80 K. A collection time of 1 or 2 hours per temperature provides good statistics.

No temperature dependence in the scattering patterns could be detected. The inset to Fig. 1 shows SANS patterns at 3 K and 30 K with incident beam parallel to the (001) direction. Intensity at 3 and 30 K in the rectangular box on the SANS pattern is shown in the main frame.

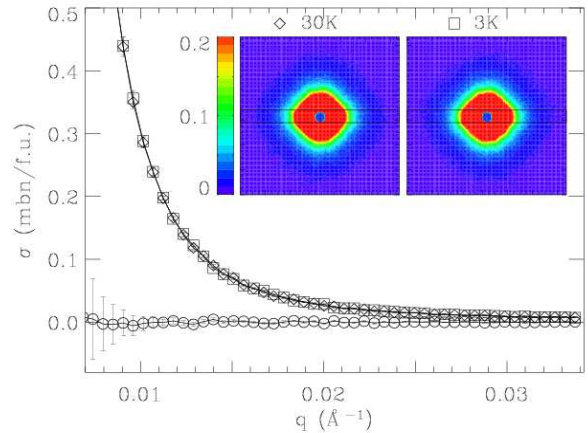


FIG. 1: (color) Measured SANS cross-section in the 10 pixels wide rectangle shown in the inset at 3 K (squares) and 30 K (diamonds), and the difference of the intensity between 3 K and 30 K (circles) as a function of wave vector transfer q . Lines are guide to the eye. Inset: the SANS pattern at 30 and 3 K, with the intensity color scale at the left.

The difference intensity (circles) fluctuates around zero, and its standard deviation sets an upper limit of 1.5×10^{-7} bn or $1.4 \times 10^{-3} \mu_B$ per Cu for ferromagnetic moments in the clusters.

This result provides serious constrain on the class of theoretical models for the spin-glass transition in doped cuprates¹⁹ which lead to formation of ferromagnetic clusters. Instead of this “large spin fixed point”, models leading to other fixed points such as “Griffiths fixed point” as discussed by Lin et al.²⁸ may be considered.

IV. TRIPLE-AXIS NEUTRON SCATTERING

While no appreciable ferromagnetic signal was detected for $\text{La}_2\text{Cu}_{0.94}\text{Li}_{0.06}\text{O}_4$, as in other Li-doped La_2CuO_4 ^{26,29}, antiferromagnetic scattering was readily observed along the rods perpendicular to the CuO_2 plane and intercepting the plane at the commensurate (π, π) -type Bragg points of the square lattice. This means that antiferromagnetic correlations in the CuO_2 plane are chessboard-like, which is similar to electron-doped La_2CuO_4 ^{30,31}, but different from the more complex, incommensurate ones in $\text{La}_{2-x}\text{Sr}_x\text{CuO}_4$ at similar hole doping³².

Scans through such a rod in the CuO_2 plane at various temperatures with the SPINS spectrometer set at $E=0$ are shown in Fig. 2(a). Inelastic scans have been reported previously in a related but different study which focuses on scaling in different quantum regimes²⁵. There is little change in the peak width in these scans, consistent with previous results of temperature independent in-plane correlation length for $\text{La}_2\text{Cu}_{0.95}\text{Li}_{0.05}\text{O}_4$ ¹ and $\text{La}_{2-x}\text{Sr}_x\text{CuO}_4$ ($0.02 \leq x \leq 0.04$)³³ below 300 K. Mod-

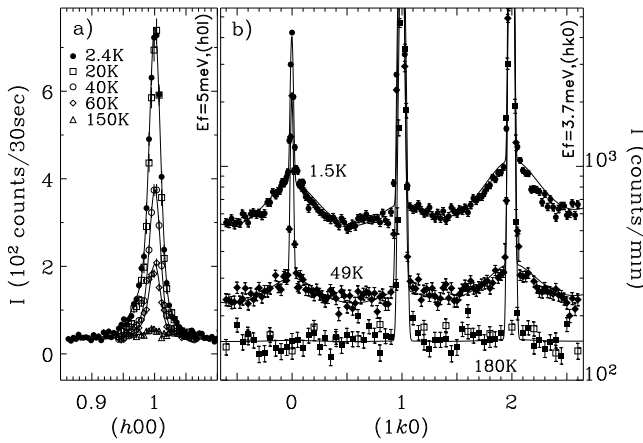


FIG. 2: Representative magnetic quasielastic and elastic scattering along a) an in-plane direction and b) the interlayer direction between 1.5 and 180 K. Open squares in b) were measured at $(1.06, k, 0)$ and represent background. The solid lines are resolution convoluted $S^{3D}(\mathbf{q}, E) + S^{q3D}(\mathbf{q}, E)$ in Eq. (3)-(4).

eling the width of the rod in Fig. 2(a) with Lorentzian

$$\mathcal{L}^\xi(q) = \frac{\xi}{\pi[1 + (q\xi)^2]}, \quad (1)$$

the *lower limits* from deconvolution is $\xi_\square \geq 274\text{\AA}$, where the \square indicates the correlation length as in-plane. These large antiferromagnetic clusters in the CuO_2 plane correlate in three different ways in the interlayer direction, giving rise to almost 3D, quasi-3D and 2D magnetic correlations. Let us now examine the three components.

Scans along the rod in the interlayer direction, with the SPINS spectrometer set at $E=0$, were measured at various temperatures from 1.5 to 180 K. A few of them, at 1.5, 49 and 180 K, respectively, are shown in Fig. 2(b). Magnetic intensity is composed of both broad and sharp peaks at magnetic Bragg points (100) and (120) of the parent compound. The (110) peak is temperature-independent thus nonmagnetic. Fitting the broad peaks to Eq. (1), we obtained an interlayer correlation length $\xi^{q3D} = 6.2(4)$ \AA . Again, no temperature dependence can be detected for ξ^{q3D} below 49 K. Above 49 K, signal is too weak to have a reliable determination of ξ^{q3D} . Thus, the quasi-3D spin correlations are typically three planes thick. For the sharp peak at (100) or (120) , only the *lower limit* for the correlation length can be reliably estimated: $\xi^{3D} \geq 168\text{\AA}$, since the width is close to instrumental resolution. Therefore, the number of correlated antiferromagnetic planes is more than 50, resembling a 3D antiferromagnetic order.

Both the broad and sharp peaks in Fig. 2(b) are energy-resolution-limited with the half-width-at-half-maximum = 0.07 meV. The energy scan in Fig. 3 is an example and more can be found in Fig. 2 in reference [25]. However, these peaks should not be regarded automatically as from *static* magnetic order. Static mag-

netic signal was observed only below $T_g=8$ K at the spin glass transition in μSR study⁶, which has a much better energy resolution. Thus, the quasi-3D and almost 3D correlations are slowly dynamic for $T > 8$ K, with their spectra faster than 1 MHz^{6,13}, the zero-field μSR static cutoff frequency, but slower than 17 GHz=0.07 meV/h, the frequency resolution at spectrometer SPINS.

The 2D antiferromagnetic correlations have been investigated in detail²⁵. The dynamic magnetic structure factor,

$$S^{2D}(\mathbf{q}, E) = \sum_{\tau} \mathcal{L}^{\xi_\square}(\boldsymbol{\kappa}_\square) \frac{\chi''(E)}{\pi(1 - e^{-\hbar\omega/k_B T})}, \quad (2)$$

where τ is a magnetic Bragg wave-vector and $\boldsymbol{\kappa} \equiv \mathbf{q} - \tau$, has been determined from measurements in the energy range, $E \leq 4.2$ meV, between 1.5 and 150 K. Eq. (2) is independent of k , befitting to a 2D magnetic correlation, see the flat k scan at 1.2 meV in Fig. 3. The almost 3D and quasi-3D spin correlations described in previous paragraphs can be written as

$$S^{3D}(\mathbf{q}, E) = I^{3D} \sum_{\tau} \mathcal{L}^{\xi_\square}(\boldsymbol{\kappa}_\square) \mathcal{L}^{\xi^{3D}}(k - \tau_k) \mathcal{L}^{1/\epsilon}(E) \quad (3)$$

and

$$S^{q3D}(\mathbf{q}, E) = I^{q3D} \sum_{\tau} \mathcal{L}^{\xi_\square}(\boldsymbol{\kappa}_\square) \mathcal{L}^{\xi^{q3D}}(k - \tau_k) \mathcal{L}^{1/\epsilon}(E), \quad (4)$$

respectively, where $\epsilon < 0.07$ meV, the spectrometer energy resolution. Note that we use conventional Lorentzian function, Eq. (1), to model sharp peaks which we could not experimentally resolve, in addition to $\mathcal{L}^{\xi^{q3D}}$ in Eq. (4) which we could resolve. We are fully aware that the true peak profile can be different for these unresolved peaks. The use of Eq. (1) is for the purpose of calculating resolution convolution of Eq. (2)-(4), which is used in the following paragraphs to obtain correct normalization of I^{2D} , I^{q3D} and I^{3D} . The choice of the function will not affect the result as long as the function describes a sharp peak significantly narrower than instrument resolution.

With negligible ferromagnetic correlations, the total dynamic structure factor is a summation of Eq. (2)-(4),

$$S(\mathbf{q}, E) = S^{2D}(\mathbf{q}, E) + S^{q3D}(\mathbf{q}, E) + S^{3D}(\mathbf{q}, E). \quad (5)$$

Of the four variables of $S(\mathbf{q}, E)$, \mathbf{q}_\square are fixed at the (π, π) -type Bragg points by the sharply peaked $\mathcal{L}^{\xi_\square}(\boldsymbol{\kappa}_\square)$ ³⁴. To comprehend the composition of $S(\mathbf{q}, E)$, it is sufficient to plot $S(\mathbf{q}, E)$ as a function of E and the interlayer wavenumber k . Such a plot of measured $S(\mathbf{q}, E)$ at 1.5 K is shown with a logarithmic intensity scale in Fig. 3. The temperature and \mathbf{q} independent incoherent scattering and other background at $E = 0$ has been subtracted, which can be determined, e.g., by the 180 K scan in Fig. 2(b). The sharp peak fitted by the red curve is from $S^{3D}(\mathbf{q}, E)$, the narrow blue ridge at $E=0$ from $S^{q3D}(\mathbf{q}, E)$, and the green surface from $S^{2D}(\mathbf{q}, E)$. The red peak at (100) is about one order of magnitude

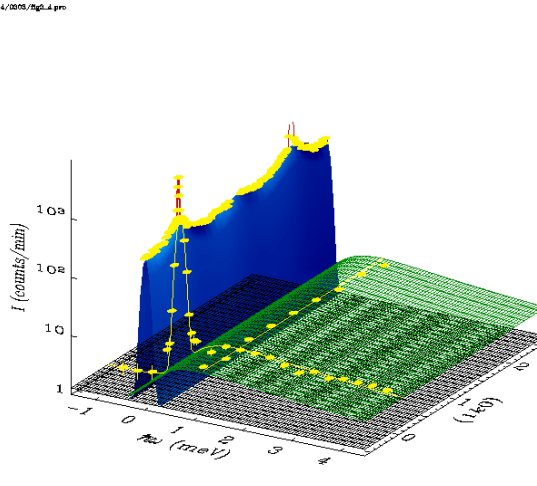


FIG. 3: (color) Measured $S(\mathbf{q}, E)$ as a function of E and interlayer k at 1.5 K with a logarithmic intensity scale, showing three color-coded magnetic components in Eq. (5). $S^{3D}(\mathbf{q}, E)$ (red) and $S^{q3D}(\mathbf{q}, E)$ (blue) are energy-resolution limited at $E = 0$, representing very slow spin dynamics which is associated with the spin-glass freezing. They are modulated along the interlayer k direction. The spin-liquid component, $S^{2D}(\mathbf{q}, E)$ (green), has a finite energy scale of about 1 meV below 50 K, and $0.18k_B T$ above 50 K²⁵. It is flat along the k direction. A few representative scans at 1.5 K are shown with yellow symbols. The black surface indicates background of ~ 1.3 counts/min.

stronger than the peak intensity of the blue surface, and three orders of magnitude stronger than the peak intensity of the green surface. Thus, $S^{3D}(\mathbf{q}, E)$ is the easiest component to be observed in a neutron scattering experiment, and is often mistakenly attributed to a *static* magnetic order.

The spectral weights $\int d\mathbf{q}dE S^{3D}(\mathbf{q}, E) \equiv I^{3D}$ and $\int d\mathbf{q}dE S^{q3D}(\mathbf{q}, E) \equiv I^{q3D}$ can be obtained by fitting resolution-convoluted Eq. (3)-(4) to scans such as those shown in Fig. 2(b). They are shown as a function of temperature in Fig. 4, with I^{3D} magnified by a factor of 5 for clarity. For the 2D component, the spectral weight is

$$I^{2D} \equiv \int dE \frac{2\chi''(E)}{\pi(1 - e^{-\hbar\omega/k_B T})}, \quad (6)$$

where the integration limits are $\pm\infty$. Green squares in Fig. 4 represent the lower bound of I^{2D} with the energy integration limited in $|E| \leq 10$ meV, using the analytical expression of $\chi''(E)$ in reference [25] to extrapolate to $E=10$ meV, where spin fluctuations were observed in $\text{La}_2\text{Cu}_{0.9}\text{Li}_{0.1}\text{O}_4$ using a thermal neutron spectrometer²⁹.

I^{3D} and I^{q3D} appear simultaneously below ~ 150 K. Their concave shape in Fig. 4 differ drastically from the usual convex-shape of a squared order parameter, orange circles, which was observed in μSR study below $T_g=8$ K⁶. They are typical neutron scattering signal from slow *dynamic* spin correlations in spin-glasses^{27,35}, which fluctuate in the frequency window between 1 MHz and 17

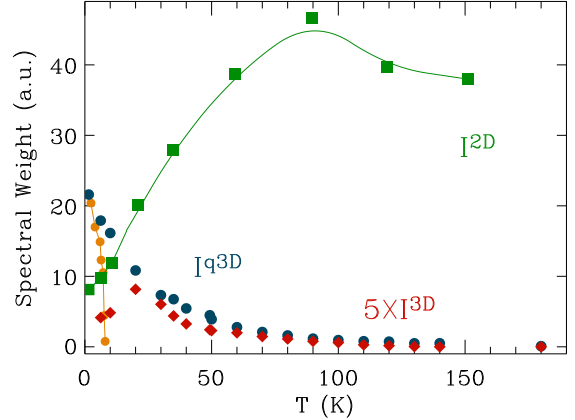


FIG. 4: (color) Temperature dependence of spectral weights I^{2D} (green), I^{q3D} (blue) and I^{3D} (red) in the same unit for three experimentally separable antiferromagnetic components in Eq. (5). $I^{3D} + I^{q3D}$ is the total spectral weight of the spin-glass component. I^{2D} is the spectral weight of the spin-liquid component within $|E| < 10$ meV, thus the lower limit of its total spectral weight. The orange circles represent squared *static* order parameter of the spin-glass transition, which was measured by μSR ⁶ and equals to $I^{3D} + I^{q3D}$ at $T=0$.

GHz for $T > 8$ K, and below 1 MHz for $T < 8$ K. Previously, energy-resolution-limited neutron scattering from $\text{La}_{1.94}\text{Sr}_{0.06}\text{CuO}_4$ was observed to have a similar temperature dependence as I^{3D} in Fig. 4 and was attributed to spin freezing¹³. The kink of I^{3D} at 20 K reflects an increased T_g from 8 K to 20 K when probing frequency is increased from 1 MHz to 17 GHz^{13,18}. At 0 Hz, $T_g \approx 6$ K from DC magnetization measurements¹¹. The increase of T_g with measurement frequency is a hallmark of glassy systems¹⁸.

V. DISCUSSIONS AND SUMMARY

The fact that I^{3D} decreases below $T_g(17\text{GHz}) \approx 20$ K while I^{q3D} continues to increase indicates that the “Edwards-Anderson order parameter”^{18,27,35} distributes only along lines such as the $(1k0)$. In conventional spin-glasses, the “Edwards-Anderson order parameter” is more isotropically distributed in the \mathbf{q} -space^{18,27,35}. Thus, the spin-glass state in $\text{La}_2\text{Cu}_{0.94}\text{Li}_{0.06}\text{O}_4$ is characterized mainly by interlayer disorder which upsets phase correlation between large antiferromagnetic clusters in different CuO_2 planes. This picture offers a possible alternative to the conventional competing antiferromagnetic/ferromagnetic interaction model for spin freezing in doped cuprates. In addition, it suggests that the weak interlayer exchange interaction likely plays an important role in the finite temperature spin-glass transition in the quasi-2D Heisenberg magnetic systems.

Another important difference from conventional spin-glasses in which all spins are believed to freeze at low

temperature is that only a fraction of spins freeze in $\text{La}_2\text{Cu}_{0.94}\text{Li}_{0.06}\text{O}_4$. Other spins in 2D correlations remain fluctuating down to 1.5 K. This is consistent with numerical evidence that quantum fluctuations prevent spin-glass transition for 2D $S=1/2$ Heisenberg system³⁶. The spin-glass component in our sample has to acquire interlayer correlations to achieve a higher dimension in order to be realized. It appears that the lower critical dimension for a $S=1/2$ Heisenberg quantum spin glass is between 2 and 3.

A further difference from conventional spin-glasses, for which one can measure the narrowing of magnetic spectrum toward $E=0$ ²⁷, is that when $S^{3D}(\mathbf{q}, E)$ and $S^{q3D}(\mathbf{q}, E)$ in $\text{La}_2\text{Cu}_{0.94}\text{Li}_{0.06}\text{O}_4$ become detectable at about 150 K, they are already energy-resolution-limited, with spins fluctuating much slower than 17 GHz. This property of $S^{3D}(\mathbf{q}, E)$ and $S^{q3D}(\mathbf{q}, E)$ resembles the classic central peak phenomenon in the soft phonon transition^{37,38}. The disparate dynamics of the central peak and phonon are explained by Halperin and Varma³⁹ using a phase separation model: defect cells contribute to the slow relaxing central peak while coherent lattice motions (phonons) to the resolved inelastic channel. This mechanism has been applied with success to a wide class of disordered relaxor ferroelectrics^{40,41}.

For $\text{La}_2\text{Cu}_{0.94}\text{Li}_{0.06}\text{O}_4$, we envision that disorder accompanying doping prevents the long-range order of the antiferromagnetic phase mainly by upsetting interlayer magnetic phase coherence, see Fig. 3 for the \mathbf{q} -distribution of frozen spins. This upsetting is not uniform in the Griffiths fashion⁴² with weak and strong coupling parts in the sample. In our laminar material, however, the weak and strong coupling parts have different dimensionality: 2D and nearly 3D, respectively. The 2D part is a spin liquid and represents essentially the whole system at high temperature, see Fig. 4. Part of sample with stronger interplane coupling tends to order three dimensionally below ~ 150 K, producing $S^{3D}(\mathbf{q}, E)$ and $S^{q3D}(\mathbf{q}, E)$. The condensation of the 2D spin liquid at ~ 150 K into the quasi-3D dynamic clusters of diminishing energy scale, instead of a true long-range order, may reflect the divergent fluctuations which destabilize static order at finite temperature for 2D random XY or Heisenberg systems^{36,43,44}. The nearly 3D spin-glass instead of a 3D antiferromagnet finally orders at a much

reduced $T_g \approx 20$ K, when $I^{q3D} + I^{3D}$ approaches the 2D spectral weight (Fig. 4). The coexistence of spin liquid and spin glass components at low temperatures may be a general consequence of no “mobility edge” separating finite and infinite range correlations for a 2D random system⁴³. Recently, Monte-Carlo simulations of a doped 2D classical antiferromagnet suggest that there are two populations of spins: one with fast and the other with slow dynamics⁴⁵. This is consistent with our experimental results and the Griffiths picture for random magnetic systems. A phenomenological Halperin and Varma model may be built for spin dynamics in doped cuprates based on these microscopic insights.

In summary, spins in $\text{La}_2\text{Cu}_{0.94}\text{Li}_{0.06}\text{O}_4$ develop *dynamic* antiferromagnetic order in the CuO_2 plane with very long ξ_{\square} below 180 K. The characteristic energy of the 2D spin fluctuations is $0.18k_B T$ for $T > 50$ K and 1 meV for $T < 50$ K²⁵. Below ~ 150 K, interlayer phase coherence appears between some of these planar antiferromagnetic clusters with an energy scale smaller than 70 μeV . While the 2D antiferromagnetic correlations in an individual plane remain liquid down to 1.5 K, coherent multiplane antiferromagnetic correlations become frozen below T_g . The phase separation into 2D spin-liquid and spin-glass of higher dimension with an unusual \mathbf{q} -structure for the “Edwards-Anderson order parameter” is most likely related to quasi-2D nature of magnetic exchange in the cuprates and is distinctly different from conventional spin-glasses.

A theory of spin-glass in doped cuprates should include interlayer coupling. Theory explaining both the partial spin freezing and the observed crossover^{25,26} of quantum spin fluctuations are called for. The heterogeneous magnetic correlations, instead of a uniform magnetic phase, suggests the possibility that superconductivity and the almost 3D antiferromagnetic order may reside in different phases in $\text{La}_{2-x}\text{Sr}_x\text{CuO}_4$ and $\text{Y}_{1-x}\text{Ca}_x\text{Ba}_2\text{Cu}_3\text{O}_{6+y}$. Similar, detailed \mathbf{q} , E and T dependent cold neutron spectroscopic study on these cuprates are desirable.

We thank R.H. Heffner, P.C. Hammel, S.M. Shapiro, C. Broholm, L. Yu, Z.Y. Weng, A.C. Castro Neto, O. Sushkov, J. Ye, F.C. Zhang, X. G. Wen, T. Senthil, P. C. Dai and C.M. Varma for useful discussions. SPINS and NG7-SANS at NIST are supported partially by NSF. Work at LANL is supported by U.S. DOE.

* Electronic address: wbao@lanl.gov

¹ Y. Endoh, K. Yamada, R. J. Birgeneau, D. R. Gabbe, H. P. Janssen, M. A. Kastner, C. J. Peters, P. J. Picone, T. R. Thurston, J. M. Tranquada, et al., *Phys. Rev. B* **37**, 7443 (1988).

² S. Chakravarty, B. I. Halperin, and D. R. Nelson, *Phys. Rev. Lett.* **60**, 1057 (1988).

³ S. Sachdev and J. Ye, *Phys. Rev. Lett.* **69**, 2411 (1992).

⁴ H. Takagi, T. Ido, S. Ishibashi, M. Uota, S. Uchida, and Y. Tokura, *Phys. Rev. B* **40**, 2254 (1989).

⁵ T. Nagano, Y. Tomioka, Y. Nakayama, K. Kishio, and K. Kitazawa, *Phys. Rev. B* **48**, 9689 (1993).

⁶ R. H. Heffner, D. E. MacLaughlin, G. J. Nieuwenhuys, J. L. Sarrao, and J. E. Sonier, *Physica B* **312**, 65 (2002).

⁷ M. Hücker, V. Kataev, J. Pommer, J. Harass, A. Hosni, C. Pfletsch, R. Gross, and B. Buchner, *Phys. Rev. B* **59**, R725 (1999).

⁸ S. Haas, F.-C. Zhang, F. Mila, and T. M. Rice, *Phys. Rev. Lett.* **77**, 3021 (1996).

⁹ C. Timm and K. H. Bennemann, *Phys. Rev. Lett.* **84**, 4994

(2000).

¹⁰ B. J. Suh, P. C. Hammel, Y. Yoshinari, J. D. Thompson, J. L. Sarrao, and Z. Fisk, Phys. Rev. Lett. **81**, 2791 (1998).

¹¹ T. Sasagawa, P. K. Mang, O. P. Vajk, A. Kapitulnik, and M. Greven, Phys. Rev. B **66**, 184512 (2002).

¹² D. R. Harshman, G. Aeppli, G. P. Espinosa, A. S. Cooper, J. P. Remeika, E. J. Ansaldo, T. M. Riseman, D. L. Williams, D. R. Noakes, B. Ellman, et al., Phys. Rev. B **38**, R852 (1988).

¹³ B. J. Sternlieb, G. M. Luke, Y. J. Uemura, T. M. Riseman, J. H. Brewer, P. M. Gehring, K. Yamada, Y. Hidaka, T. Murakami, T. R. Thurston, et al., Phys. Rev. B **41**, 8866 (1990).

¹⁴ F. C. Chou, F. Borsa, J. H. Cho, D. C. Johnston, A. Lascialfari, D. R. Torgeson, and J. Ziolo, Phys. Rev. Lett. **71**, 2323 (1993).

¹⁵ C. Niedermayer, C. Bernhard, T. Blasius, A. Golnik, A. Moodenbaugh, and J. I. Budnick, Phys. Rev. Lett. **80**, 3843 (1998).

¹⁶ C. Panagopoulos, A. P. Petrovic, Hillier, J. L. Tallon, C. A. Scott, and A. P. Rainford, Phys. Rev. B **69**, 144510 (2004).

¹⁷ F. C. Chou, N. R. Belk, M. A. Kastner, R. J. Birgeneau, and A. Aharony, Phys. Rev. Lett. **75**, 2204 (1995).

¹⁸ K. Binder and A. P. Young, Rev. Mod. Phys. **58**, 801 (1986).

¹⁹ R. J. Gooding, N. M. Salem, R. J. Birgeneau, and F. C. Chou, Phys. Rev. B **55**, 6360 (1997).

²⁰ N. Hasselmann, A. H. C. Neto, and C. M. Smith, Phys. Rev. B **69**, 014424 (2004).

²¹ S. P. Kou and Z. Y. Weng, Phys. Rev. Lett. **90**, 157003 (2003).

²² O. Sushkov and A. Castro-Neto, e-print cond-mat/0504234.

²³ P. A. Marchetti, L. DeLeo, G. Orso, Z. B. Su, and L. Yu, Phys. Rev. B **69**, 024527 (2004).

²⁴ P. A. Marchetti, G. Orso, Z. B. Su, and L. Yu, Phys. Rev. B **69**, 214514 (2004).

²⁵ W. Bao, Y. Chen, Y. Qiu, and J. L. Sarrao, Phys. Rev. Lett. **91**, 127005 (2003).

²⁶ Y. Chen, W. Bao, J. E. Lorenzo, A. Stunault, J. L. Sarrao, S. Park, and Y. Qiu, e-print cond-mat/0408547.

²⁷ K. Motoya, S. M. Shapiro, and Y. Muraoka, Phys. Rev. B **28**, 6183 (1983).

²⁸ Y.-C. Lin, R. Mélin, H. Rieger, and F. Iglói, Phys. Rev. B **68**, 24424 (2003).

²⁹ W. Bao, R. J. McQueeney, R. Heffner, J. L. Sarrao, P. Dai, and J. L. Zarestky, Phys. Rev. Lett. **84**, 3978 (2000).

³⁰ K. Yamada, K. Kurahashi, T. Uefuji, M. Fujita, S. Park, S.-H. Lee, and Y. Endoh, Phys. Rev. Lett. **90**, 137004 (2003).

³¹ H. J. Kang, P. Dai, H. A. Mook, D. N. Argyriou, V. Sikolenko, J. W. Lynn, Y. Kurita, S. Komiya, and Y. Ando, Phys. Rev. B **71**, 214512 (2005).

³² M. Fujita, K. Yamada, H. Hiraka, P. M. Gehring, S. H. Lee, S. Wakimoto, and G. Shirane, Phys. Rev. B **65**, 64505 (2002).

³³ B. Keimer, N. Belk, R. J. Birgeneau, A. Cassanho, C. Y. Chen, M. Greven, M. A. Kastner, A. Aharony, Y. Endoh, R. W. Erwin, et al., Phys. Rev. B **46**, 14034 (1992).

³⁴ Instrumental in-plane \mathbf{q} resolution varies at different (\mathbf{q}, E) for spectra in Eq. (2-4). Thus, the lower limits are $\xi_{\square} \geq 274 \text{ \AA}$ from scan at (100) and $E = 0$, $\xi_{\square} \geq 70 \text{ \AA}$ from scan at (1,0,4,0) and $E = 0$, and $\xi_{\square} \geq 55 \text{ \AA}$ at finite E .

³⁵ A. P. Murani and A. Heidemann, Phys. Rev. Lett. **41**, 1402 (1978).

³⁶ R. N. Bhatt and P. A. Lee, Phys. Rev. Lett. **48**, 344 (1982).

³⁷ S. Shapiro, J. D. Axe, G. Shirane, and T. Riste, Phys. Rev. B **6**, 4332 (1972).

³⁸ T. Riste, E. J. Samuelsen, K. Otnes, and J. Feder, Solid State Comm. **9**, 1455 (1971).

³⁹ B. I. Halperin and C. M. Varma, Phys. Rev. B **14**, 4030 (1976).

⁴⁰ E. Courtens, J. Phys. (France) **43**, L199 (1982).

⁴¹ G. Burns and F. H. Dacol, Phys. Rev. B **28**, 2527 (1983).

⁴² H. Rieger and A. P. Young, in *Complex Behaviour of Glassy Systems*, edited by J. M. Rubí and C. Pérez-Vicente (Springer, Berlin, 1997), p. 256.

⁴³ J. A. Hertz, L. Fleishman, and P. W. Anderson, Phys. Rev. Lett. **43**, 942 (1979).

⁴⁴ L.-H. Tang and P. Tong, Phys. Rev. Lett. **94**, 207204 (2005).

⁴⁵ M. P. Kennett, C. Chamon, and L. F. Cugliandolo, Phys. Rev. B **72**, 024417 (2005).